

# Elicitation of FANO resonances and confinement well using pattern recognition over UV-Vis spectra of gold nano spheres

M. F. YILMAZ<sup>1,\*</sup>, M. OZDEMIR<sup>1</sup>, Y. DANISMAN<sup>2</sup>, B. KARLIK<sup>3</sup> and O. O. AGA<sup>4</sup>

<sup>1</sup>Basic Sciences, College of Engineering, Imam Abdulrahman Bin Faisal university, P.O. Box 1982, Dammam, 31451, SA

<sup>2</sup>Department of Mathematics and Computer Sciences, Queensborough Community College, CUNY, Bayside, NY, USA

<sup>3</sup>Neurosurgical Simulation and Artificial Intelligence Learning Centre, Montreal Neurological Institute, McGill University, H3A2B4, Montreal, QC, CANADA

<sup>4</sup>Environmental Engineering, College of Engineering, Imam Abdulrahman Bin Faisal university, P.O. Box 1982, Dammam, 31451, SA

\*Correspondence to [fhylmaz53@gmail.com](mailto:fhylmaz53@gmail.com)

## Abstract

Here, we have employed Principal Component Analysis (PCA) and Linear Discriminant Analysis (LDA) to analyze a database consisting of Mie calculated UV-Vis spectra of gold nanospheres (GNS). PCA and LDA extract the hidden structures of the database by the corresponding vectors and coordinates. 3D representation of coordinates of PCA of spectral database results in a beam of surface plasmon polaritons (SPP) following a parabolic trajectory. The eigen spectra of PCA exhibit the Fano type resonances of SPP, and quantum confinement effects are observed by 3D representation of LDA coordinates obtained from the database. In addition, standing wave patterns resulting from oscillations of ions and electrons are illustrated through the eigen spectra of LDA. Such results confirm that GNPs have high potential for high energy density

physics applications. Furthermore, the coordinates of PCA of spectral database are used for the training of Machine Learning (ML) algorithms for the estimation of the diameters of GNS. As a result, experimental spectra of diameters of GNS are tested, and the outputs of ML algorithms and Dynamic Light Scattering (DLS) measurements are compared for reliability of calculations. PCA based artificial neural network (ANN) were found to estimate the diameters with a high accuracy. Moreover, our results show that application of PCA and LDA on spectra could efficiently investigate the light-nanoparticles interactions for applications like rapid size determination.

## Introduction

The arrangement of metal nanoparticles in an order of chain or array provides surface plasmon polaritons (SPPs), which are the bosonic (quasiparticles) coupled modes of an incident electromagnetic wave and free electrons (plasmon) of surface. SPPs can manipulate the radiation and perform as micro-optical devices and can propagate in undistorted manner for several diffraction lengths along a metal surface [1,2 and 3]. Fano resonance stands as the primary physical mechanism behind the manipulation of electromagnetic waves [4]. Fano resonance which is obtained from sharp transmission and reflection of curves can be produced through the scattering of the electromagnetic waves by nano-particles. Besides, the fact that Fano-type shape, and remarkable strength of the observed resonance are characterized by the interaction of dielectric resonator arrays with Fabry-Perot standing waves is expressed by Semouchkina et al.,2015 [5]. The same characteristic asymmetric “Fano line shape” and coherent neutron scattering originating from standing waves in the presence of intense laser pulse with  $10^{27}$  photons/cm<sup>3</sup> can be seen by the theory of the nuclear scattering cross-section for neutron capture [6 and 7]. Kaymak et al. 2015 shown that ultra- dense high energy density plasmas ( $n_e > 9 \times 10^{24}$  cm<sup>-3</sup>) can be

generated by the irradiation of relativistic intensity femtosecond laser with aligned nanowires [8]. Beg et al., 2016 stated that there are several important properties of nano structured targets which are important for various applications such as creation of dense hot plasmas with a temperature of 2-4 keV, efficient x-ray and ion sources. [9]. Lastly, Rocca et al., 2018 has justified that array formatted nanowires completely absorb the high energy pulses and thereby producing efficient number of neutrons [10]. These capabilities of nanoparticles have strong impacts in the field of high energy density physics of fusion applications.

UV-Vis spectroscopy as a useful tool is employed for the characterization, estimation of the sizes of nanoparticles, concentration and aggregation level. It is a useful technique as UV-vis spectrometers can be found in many laboratories, the analysis does not change the sample, and the time needed for registration of the spectrum is very short. If the appropriate correction of the metal dielectric constant for the nanoparticle size and physicochemical environment is provided, then Mie theory can be used to analyze the extinction spectra of AuNP recorded by UV-vis spectroscopy [11 and 12].

On the other hand, Yilmaz et al., 2019 showed that application of PCA and LDA over the spectral database of plasma could inform more physical insight of deeper structures and polarization types of the ion species and electron ion oscillations in the plasma [12 and 13]. In addition, several reports use principal component and linear discriminant analysis (PCA and LDA) and artificial neural networks (ANN) while some of the pattern recognition techniques were used to estimate diameters of nanoparticles [14 and 15].

PCA and LDA are the two of the most common statistical techniques that are used in order to reduce the dimensions of a given raw data in pattern recognition problems. PCA uses rotational transformation in a way that most of

the data variability remains in a space of low dimensions, and it ignores the remaining dimensions that contain little variability. LDA, as a pattern recognition technique, is quite similar to that of PCA. The main difference is that, LDA determines the vectors that best separate the classes while trying to keep the variance maximum. Although it looks like LDA outperforms PCA in multi-class settings where class labels are known, it might not always be the case, especially if the sizes of the classes in the data sets are relatively small. Besides, LDA performs well only if the classes have equal covariance. PCA is good at keeping dimensions of highest variance, but it can disregard discriminant dimensions where LDA is needed. It is easy to find examples where LDA outperforms PCA and vice versa [11 and 12].

Artificial neural network (ANN) algorithms have also been of great interest and used over the last couple of decades in many applications and areas such as remote sensing, computer vision, pattern recognition and medical diagnosis. The ANN algorithms can easily identify and extract the patterns by setting correlation between sets of given inputs and outputs through a training process. Their adaptive nature especially allows solving complex and non-linear problems. Another advantage of an ML algorithm is the fact that it can establish strong correlation between the parameters without any knowledge of them. Therefore, it enables to handle uncertainties, data with noise and nonlinear relationships which are hard to determine [16,17,18, and 19]. ANNs have been applied both to X-ray spectra to predict plasma electron temperatures and densities, and to UV- Vis and FTIR spectra to investigate forensics [20 and 21]. Lately, they have been used to estimate the diameters of nanoparticles [15].

In this work, we have investigated first employed Mie scattering generated spectra of GNS as our database. This database was then analyzed by PCA and LDA methods, and the physical interpretations of PCA and LDA of

UV-Vis spectra of gold were examined. Then, the extracted PCA coordinates were used for the training of ANN to estimate the diameters of GNS. Finally, the experimental spectra of gold spheres with diameters 5, 7, 10, 15, 20 and 30 nm were tested for the estimation of diameters [22]. Our findings reveal that PCA based artificial neural network (ANN) estimates the diameters of gold nanoparticles with a remarkably high accuracy.

## Experimental

**Materials.** Hydrogen tetrachloroaurate (III) trihydrate ( $\text{HAuCl}_4 \cdot 3\text{H}_2\text{O}$ , gold salt), trisodium citrate (reducing agent), and sodium chloride were obtained from Aldrich and used as received. Gold nanoparticles (AuNPs) with the sizes of 5, 7, 10, 15, 20 and 30 nm (Fig.1) were purchased from Nanocomposix, Inc. Distilled water was used to prepare the aqueous solutions of AuNPs. Au nanoparticles were synthesized through the well-established reduction methods of Turkevich, Frens and Murphy [23, 24 and 25]. In the preparation of 5 nm AuNPs, a 10 mL aqueous solution containing 0.25 mM  $\text{HAuCl}_4$  and 0.25 mM trisodium citrate were first prepared. Ice-cooled 0.3 mL of 0.1 M sodium borohydride was added to this solution while stirring. The color change in the solution was an indication of the particle formation.

**Synthesis.** For the synthesis of 7 nm or larger AuNPs, aqueous solutions of 0.254 mM  $\text{HAuCl}_4$  and 38.8 mM trisodium citrate were first prepared. In a typical synthesis, 50 mL  $\text{HAuCl}_4$  solution was heated to boiling. After 5 min., 0.4-2.0 mL trisodium citrate solution was added to this mixture at once and the mixture was stirred for approximately 15 min. The color of the reaction mixture was turned from yellow to colorless and then ruby red color depending on the AuNPs sizes. After cooling to RT, the samples were centrifuged and washed several times with DI water to obtain 5, 7, 10, 15, and 30 nm citrate-coated AuNPs.

**Characterization.** Dynamic light scattering (DLS, Malvern Zetasizer Nano ZS) technique was used to determine the average hydrodynamic diameters of gold nanoparticles. Nano ZS detects the scattered light at an angle of  $173^\circ$ , known as backscatter detection, by using He-Ne laser (4 mW) operated at 633 nm. Aqueous 10 mM NaCl solutions were used for all DLS measurements.

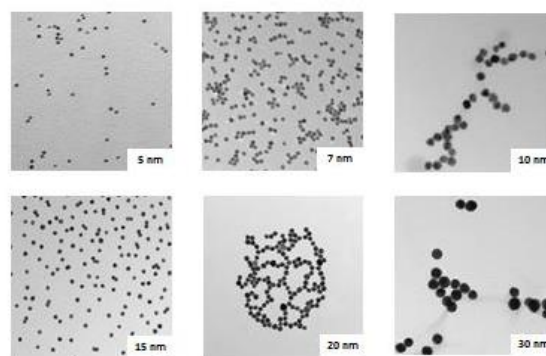


Fig. 1. TEM images of gold nanoparticles

## Mie Scattering

The Mie theory is known to be what is used for the absorption and scattering of an electromagnetic plane wave through a homogenous sphere. Although it is based on idealized initial conditions, it is widely used for the radiation problems in a light scattering media. This theory mainly calculates the coefficients for absorption, scattering and extinction. One can find several programs that can perform Mie theories-based solutions. The main advantage of the Mie methods is that they suggest solutions for the cases where the diameter of scattering particle is comparable to the wavelength of the light. For much larger or smaller particle sizes, there are already several simple methods that can be used in order to describe the behavior of the corresponding systems. Since our focus is on the sizes similar to the incoming light wavelength, we employed Mie theory calculated spectra to create our database [26 and 27]. Our database contains 25 spectra of gold spheres without polymer shell with the diameters 2, 4, 6, ..., 50 nm. In Fig.2,

experimental spectra of 5, 7, 10, 15 and 30 nm and their Mie calculated spectra are illustrated. By applying PCA to the whole database, eigenvalues with corresponding eigenvectors of the covariance matrix are obtained. Throughout this work, only the first three eigenvectors, which correspond to the largest three eigenvalues, are considered to reduce the dimension of the initial.

The Mie theory we used in this work employs the spherical vector harmonics to express the electromagnetic fields in the form of scattered shape for the dipole interactions. Vector-basis functions,—are derived from the separable solutions to the scalar Helmholtz equation. The relative intensity of the scattering or absorption of particles with different sizes is described by the particle efficiency which *is* calculated by dividing the scattering/absorption/extinction cross section by the geometrical cross-sectional area. These cross sections are obtained by the integration of the Poynting vector for a spherical radius. The experimental size dependent dielectric electric effects in gold nanoparticles is described by a Drude conduction model. In addition, enhancement of the local intense fields due to the presence of local surface roughness are described by amplification mechanisms in the model [22, 26 and 27].-

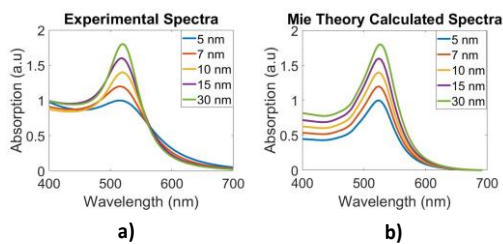


**Fig. 2.** a) Experimental UV-Vis spectra and b) Mie calculated spectra

### Principal Component Analysis (PCA)

The main purpose of PCA is to find a subspace spanned by the vectors with largest variances. This is an optimization problem, which reduces

the dimension of a data set while retaining the variance. This goes through by converting the data set of possibly correlated variables into linearly uncorrelated variables called Principal Components (PC). These PCs determine the similarities and differences of the data, and they are the eigenvectors of the covariance matrix which consists of covariances of all different dimensions. Hence, every element of the original data can be written as a linear combination of PCs. To reduce the dimension, only the eigenvectors ( $|PC1\rangle$ ,  $|PC2\rangle$  and  $|PC3\rangle$  in this paper) which correspond to the largest (dominant) eigenvalues of the covariance matrix are considered. The original data is projected into the space spanned by these PCs which are orthonormal. In this way, some information is lost due to not considering the eigenvectors corresponding to the small eigenvalues, but this information has less significance [12].

Fig. 3a illustrates the 3D representation of PCA coordinates of GNS, which exhibits a parabolic trajectory. Fig. 3b illustrates the mean absorbance and vector representation of the spectra.  $|PC1\rangle$  vector spectrum represents the dipole surface Plasmon resonance, and  $|PC2\rangle$  vector spectrum which is perpendicular to the  $|PC1\rangle$  vector represents asymmetric line shape of Fano like resonance. Fano resonance which is resulted by the interference of the scattering amplitudes of continuous (bright mode) and discrete states (dark mode) provides a field enhancement. It is known that non-diffractive (airy) beam of surface Plasmon polariton (SPP) wave follows parabolic trajectory during its travel and Fano resonance originates from the coupling SPP and waveguide modes [28 and 29]. Therefore, Fig. 3 shows that, PCA can efficiently extract the propagation and resonance characteristics of the SPP over spectral database of GNS. Furthermore, SPPs are observed in the array and chain form of nanoparticles. Since our database is generated by the spectra of different diameters of gold nanospheres in ascending order, such an array behavior is expected [30].

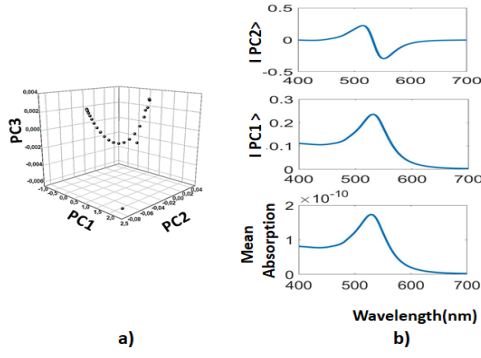


**Fig. 3.** a)  $|PC1\rangle$ ,  $|PC2\rangle$  and  $|PC3\rangle$  coordinates b) Spectra of the mean of the initial data, and first two dominant eigenvectors  $|IPC1\rangle$  and  $|IPC2\rangle$  of the covariance matrix.

### Linear Discriminant Analysis (LDA)

Similarly, to PCA, LDA is another dimension reduction technique to identify the hidden structures of large data sets [13]. LDA is applied to data sets, which consist of different classes of similar elements and used to find vectors, to discriminate the classes while respecting the similarities among the class members. On the contrary, PCA deals with the entire data, and it does not consider different classes. Therefore, LDA is applied to data sets when different classes must be considered. The eigenvectors corresponding to the largest three eigenvalues in LDA are  $|LD1\rangle$ ,  $|LD2\rangle$  and  $|LD3\rangle$ .

In Fig. 4a, LDA coordinates in 3D exhibit quantum confinement structure. Such confinements are expected as the size of the particle decreases to nanoscale comparable to the electron's wavelength. The electrons in these structures behave like a particle in potential well. Confined standing waves are the time independent solutions of the Schrodinger equations in the potential well which are formed by concurring of two anti-propagating surface plasmon waves [30 and 31]. Fig. 4b shows the LDA vector spectra which illustrate the oscillating wave pattern of ions ( $|LD1\rangle$ ) and electrons ( $|LD2\rangle$ ) [32, 33 and 34]. Fast Fourier transform modeling of ions and electrons results oscillation frequency of 31 Hz and 72 Hz, respectively.

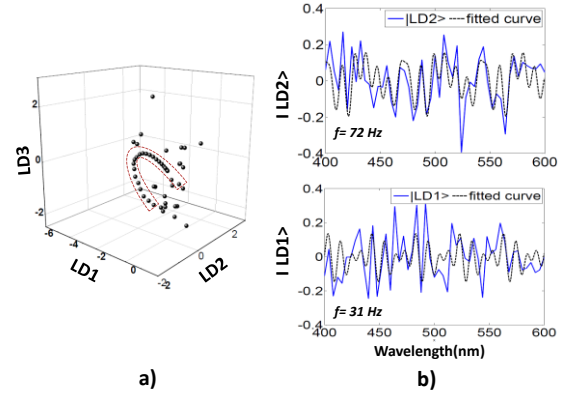


**Fig. 4.** a)  $|LD1\rangle$ ,  $|LD2\rangle$  and  $|LD3\rangle$  coordinates b) The spectra of the first two dominant eigenvectors  $|LD1\rangle$  and  $|LD2\rangle$  obtained in LDA.

### Artificial Neural Networks

Artificial Neural Network (ANN) is most popular and useful method of Machine learning algorithms. ANN is to adapt their behavior to the changing characteristics of the modeled system. As a parallel processing distributed system, artificial neural networks (ANN) depend on learning through a training set of data using a supervised learning algorithm [35]. The processing units in feed forward and back-propagation neural networks are arranged in multi layered perceptron (MLP) architectures which have back-propagation (BP) algorithm and uses various activation functions. Most commonly used non-linear activation functions are the sigmoid and the hyperbolic tangent functions [36 and 37]. As seen in Fig. 5, each layer of MLP is fully connected to the previous layer and has no other connections. The MLP consists of 3 or more layers including one input, one output and one or more hidden layers. Multiple hidden layers of non-linearly activating nodes make a deep neural network. In this study, we used four layered MLP architecture; input and output layers with one node, and hidden layers with five nodes.

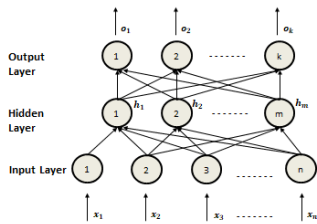


**Fig. 5.** Illustration of a general MLP architecture.

The BP with generalized delta learning rule with an iterative gradient algorithm is implemented to minimize the mean square error (MSE) between the actual output of a multilayered feed-forward neural network and a target output. MSE is also used to measure how well ANN works.

In this study, two different MLP architectures (ANN-1 and ANN2) were used. The architecture of ANN-1 is 1:25:1 which has only 1 hidden layer. The other is 1:5:5:1 which has 2 hidden layers. For both architectures, the learning rates and momentum coefficients are chosen to be 0.1 and 0.95 respectively.

Figure 6 shows that there is a nonlinear relation between the extracted PCA and LDA coordinates and the corresponding diameters. PCA coordinates which are obtained from the spectra produced from Mie scattering theory are used for the training process, and the outputs are the diameters of the nanoparticles. In this setting, it should be pointed out that PCA method provides an advantage for the use of ANNs and the other machine learning algorithms as it enables to reduce the dimension of inputs. Since LDA of spectra of GNSs reveals structures of nonlinear ion and electron oscillations (Fig. 6b), LDA based ANN was not studied in this work.

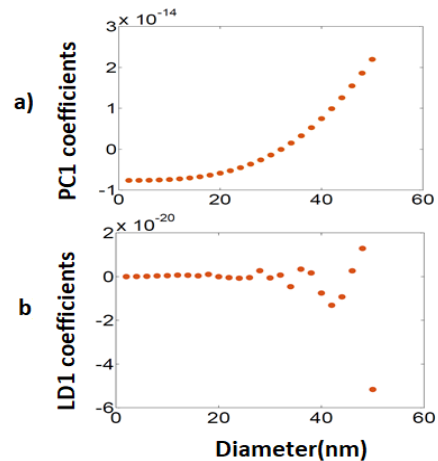


**Fig. 6.** Plot of a) |PC1> and b) |LD1> coordinates versus GNS diameters

In Table 1, Dynamic Light Scattering (DLS) measurements of gold spheres and estimations of diameters obtained by ML algorithms are compared. ANN-2, which consists of (1:5:5:1) MLP structure has shown the best recognition accuracy which is 100%. Additionally, ANN estimations show that average testing zero error was found for 6 different diameters.

NSP (nm)	DLS Diameter (nm)	ANN-1 (nm)	ANN-2 (nm)
5	5.0±0.6	7	5
7	7.5±0.8	8	7
10	11.6±1	9	10
15	15.4±1.5	13	15
20	20.5±2.1	20	20
30	31.0±3	30	30
MSE_Test_Data		1.21	0

Table 1. Values of measured and estimated diameters with error.

It is difficult to estimate IIO (one input-1 output) complicated data even if it has small-scale data which has complex convex region on the data space according to data mining rules. It is also difficult to estimate the spectra for small nanoparticles of different sizes. In this work, we have solved this problem by using multi hidden layered ANN as a deep learning algorithm. Deep learning is a class of machine learning algorithms that use a cascade of many layers of nonlinear processing units for feature extraction and transformation as in ANN-2. Each

successive layer uses the output from the previous layer as an input.

## Conclusions

Our results show that Mie calculated UV-Vis spectra can provide substantial insights of light-GNS interactions through PCA and LDA. PCA of spectral database reveals the Fano resonance characteristics of the SPP. LDA of spectra reveals the quantum confinement effects, and ion and electron oscillations. Such capabilities show that GNPs have high potentials in high energy density physics and fusion applications besides medical and industrial applications. After calculation of PCA coordinates, a nonlinear relation between the coordinates and the particle diameters is observed. It was due to the PCA coordinates that we could reduce the dimension of input data for the training of ANN, and thereby simplifying the inputs and outputs of ANN modeling. It was a rather difficult estimation because the spectra are very different for small nanoparticles. We used four well-known and effective ML algorithms and found that the most error-free result came from ANN-2. ANN-2 is, therefore, established as a powerful tool for estimating the diameters with high accuracy, since it resulted in the best recognition accuracy with a 100% by using 6 different diameters. In conclusion, a 4 layered ANN model could be suggested as a useful method for predicting the results of a proposed model in terms of saving time and cost, and that pattern recognition based multi hidden layered ANN is a powerful method for estimating the diameters of nanoparticles.

## ACKNOWLEDGEMENTS

Special thanks to Nanocomposix Inc. for providing TEM images and measurements of nanoparticles and MIE scattering calculator. for many useful discussions.

## LIST OF REFERENCES

1. Petryayeva, E. & Krull, U. J. Localized surface plasmon resonance: nanostructures, bioassays and biosensing—a review. *Analytica chimica acta*, **706(1)**, 8-24 (2011).

2. Evlyukhin, A. B., Bozhevolnyi, S. I., Stepanov, A. L., Kiyan, R., Reinhardt, C., Passinger, S. & Chichkov, B. N. Focusing and directing of surface plasmon polaritons by curved chains of nanoparticles. *Optics express*, **15(25)**, 16667-16680 (2007).
3. Salandrino, A. & Christodoulides, D. N. Airy plasmon: a nondiffracting surface wave. *Optics letters*, **35(12)**, 2082-2084 (2010).
4. Shopa, M., Kolwas, K., Derkachova, A. & Derkachov, G. Dipole and quadrupole surface plasmon resonance contributions in formation of near-field images of a gold nanosphere. *Opto-Electronics Review*, **18(4)**, 421-428 (2010).
5. Limonov, M. F., Rybin, M. V., Poddubny, A. N., & Kivshar, Y. S. (2017). Fano resonances in photonics. *Nature Photonics*, *11(9)*, 543.
6. Semouchkina, E., Duan, R., Semouchkin, G., & Pandey, R. (2015). Sensing based on Fano-type resonance response of all-dielectric metamaterials. *Sensors*, *15(4)*, 9344-9359.
7. Breit, G., & Wigner, E. (1936). Capture of slow neutrons. *Physical review*, *49(7)*, 519.
8. Stassis, C. (1973). Slow-neutron scattering by a standing electromagnetic wave. *Physical Review C*, *7(5)*, 1926.
9. Kaymak, V., Pukhov, A., Shlyaptsev, V. N., & Rocca, J. J. (2016). Nanoscale ultradense Z-pinch formation from laser-irradiated nanowire arrays. *Physical review letters*, *117(3)*, 035004.
10. Ostrikov, K. K., Beg, F., & Ng, A. (2016). Colloquium: Nanoplasmas generated by intense radiation. *Reviews of Modern Physics*, *88(1)*, 011001.
11. Curtis, A., Calvi, C., Tinsley, J., Hollinger, R., Kaymak, V., Pukhov, A., ... & Rocca, J. J. (2018). Micro-scale fusion in dense relativistic nanowire array plasmas. *Nature communications*, *9(1)*, 1077.
12. Amendola, V., & Meneghetti, M. (2009). Size evaluation of gold nanoparticles by UV-vis spectroscopy. *The Journal of Physical Chemistry C*, *113(11)*, 4277-4285.
13. Yilmaz, M. F., Danisman, Y., Ozdemir, M., Karlik, B., & Larour, J. (2019). Investigation of electron beam effects on L-shell Mo plasma produced by a compact LC generator using pattern recognition. *Matter and Radiation at Extremes*, *4(2)*, 027401.
14. Yilmaz, M. F., Danisman, Y., Larour, J., & Arantchouk, L. (2019). Linear discriminant analysis based predator-prey analysis of hot electron effects on the X-pinch plasma produced K-shell Aluminum spectra. *Scientific reports*, *9*.
15. Martínez, J. C., Chequer, N. A., González, J. L. & Cordova, T. Alternative methodology for gold nanoparticles diameter characterization using PCA technique and UV-Vis spectrophotometry. *Nanoscience and Nanotechnology*, **2(6)**, 184-189 (2012).
16. Shabanzadeh, P., Senu, N., Shameli, K., Ismail, F., Zamanian, A. & Mohagheghatabar, M. Prediction of silver nanoparticles diameter in montmorillonite/chitosan bionanocomposites by

- using artificial neural networks. *Research on Chemical Intermediates*, **41(5)**, 3275-3287 (2015).
17. Khan, I.Y., Zope, P.H., Suralkar, S.R. Importance of artificial neural network in medical diagnosis disease like acute nephritis disease and heart disease, *Int. J. Eng. Sci. Innovat. Technol.* **2**, 210-217 (2013).
  18. Guo, Y., De Jong, K., Liu, F., Wang, X. & Li, C. A comparison of artificial neural networks and support vector machines on land cover classification, in: *Proc. of the 6th Int. Symp. on Intelligence Computation and Applications ISICA, Communication in Computer and Information Science*, **316**, 531-539 (2012).
  19. Eleyan, A. & Demirel, H. PCA an LDA based face recognition using feed forward neural network classifier, multimedia content representation, classification and security, *Lect. Notes Comput. Sci.* **4105**, 199-206 (2006).
  20. Asadnia, M., Khorasani, A. M. & Warkiani, M. E. An Accurate PSO-GA Based Neural Network to Model Growth of Carbon Nanotubes. *Journal of Nanomaterials*. (2017).
  21. Yilmaz, M. F., Eleyan, A., Aranchuk, L. E. & Larour, J. Spectroscopic analysis of X-pinch plasma produced on the compact LC-generator of Ecole Polytechnique using artificial neural networks. *High Energy Density Physics*, **12**, 1-4 (2014).
  22. Wang, Q., He, H., Li, B., Lin, H., Zhang, Y., Zhang, J., & Wang, Z. (2017). UV-Vis and ATR-FTIR spectroscopic investigations of postmortem interval based on the changes in rabbit plasma. *PLoS one*, **12(7)**, e0182161.
  23. Oldenburg S.T. Light Scattering from gold nanoshells. Diss. *Rice University* (2000).
  24. Turkevich, J., Stevenson, P. C. & Hillier, J. A study of the nucleation and growth processes in the synthesis of colloidal gold. *Discussions of the Faraday Society*, **11**, 55-75 (1951).
  25. Frens, G. Controlled nucleation for the regulation of the particle size in monodisperse gold suspensions. *Nature physical science*, **241**, 20-22 (1973).
  26. Jana, N. R., Gearheart, L. & Murphy, C. J. Seeding growth for size control of 5- 40 nm diameter gold nanoparticles. *Langmuir*, **17(22)**, 6782-6786 (2001).
  27. Sarkar, D., & Halas, N. J. General vector basis function solution of Maxwell's equations. *Physical Review E*, **56(1)**, 1102 (1997).
  28. Oldenburg, S. J., Averitt, R. D., Westcott, S. L., & Halas, N. J. Nanoengineering of optical resonances. *Chemical Physics Letters*, **288(2-4)**, 243-247 (1998).
  29. Zhu, Z., Bai, B., You, O., Li, Q. & Fan, S. Fano resonance boosted cascaded optical field enhancement in a plasmonic nanoparticle-in-cavity nanoantenna array and its SERS application. *Light: Science & Applications*, **4(6)**, e296 (2015).
  30. Kong, X., Qiu, L. & Xiao, G. Fano resonance in high-permittivity objects. *In Resonance. InTech* (2017).
  31. Li, L., Li, T., Wang, S. M., Zhang, C. & Zhu, S. N. Plasmonic airy beam generated by in-plane diffraction. *Physical review letters*, **107(12)**, 126804 (2011).
  32. Sekkat, Z., Hayashi, S., Nesterenko, D. V., Rahmouni, A., Ishitobi, H., Inouye, Y., & Kawata, S. Fano resonances arising from coupled surface plasmon polariton and waveguide modes (Conference Presentation). *Plasmonics: Design, Materials, Fabrication, Characterization, and Applications XIV International Society for Optics and Photonics*, **9921**, 99210K (2016).
  33. Jacak, W. A. On plasmon polariton propagation along metallic nano-chain. *Plasmonics*, **8(3)**, 1317-1333 (2013).
  34. Crommie, M. F., Lutz, C. P. & Eigler, D. M. Confinement of electrons to quantum corrals on a metal surface. *Science*, **262(5131)**, 218-220 (1993).
  35. Fang, Y. & Tian, X. Resonant surface plasmons of a metal nanosphere can be considered in the way of propagating surface plasmons. *arXiv preprint arXiv:1412.2664*, (2014).
  36. Kizilaslan, R., & Karlik, B. Combination neural networks forecasters for monthly natural gas consumption prediction. *Neural Network World*, **19(2)**, 191-199 (2009).
  37. Karlik, B., & Olgac, A.V. Performance analysis of various activation functions in generalized MLP architectures of neural networks. *International Journal of Artificial Intelligence and Expert Systems*. **1(4)**, 111-122 (2011).
  38. Karlik, B. A neural network image recognition for control of manufacturing plant. *Mathematical & Computational Applications*. **8(2)**, 181-189 (2003).